

A Steering Paradox for Einstein-Podolsky-Rosen Argument and its Extended Inequality

Tianfeng Feng,¹ Changliang Ren,^{2,*} Qin Feng,¹ Maolin Luo,¹ Xiaogang Qiang,³ Jing-Ling Chen,^{4,†} and Xiaoqi Zhou^{1,‡}

¹State Key Laboratory of Optoelectronic Materials and Technologies and School of Physics,
Sun Yat-sen University, Guangzhou, People's Republic of China

²Key Laboratory of Low-Dimensional Quantum Structures and Quantum Control of Ministry of Education,
Key Laboratory for Matter Microstructure and Function of Hunan Province,
Department of Physics and Synergetic Innovation Center for Quantum Effects
and Applications, Hunan Normal University, Changsha 410081, China

³National Innovation Institute of Defense Technology, AMS, Beijing, China

⁴Theoretical Physics Division, Chern Institute of Mathematics,
Nankai University, Tianjin 300071, People's Republic of China

(Dated: May 3, 2021)

The Einstein-Podolsky-Rosen (EPR) paradox is one of the milestones in quantum foundations, arising from the lack of local realistic description of quantum mechanics. The EPR paradox has stimulated an important concept of “quantum nonlocality”, which manifests itself by three different types: quantum entanglement, quantum steering, and Bell nonlocality. Although Bell nonlocality is more often used to show the “quantum nonlocality”, the original EPR paradox is essentially a steering paradox. In this work, we formulate the original EPR steering paradox into a contradiction equality, thus making it amenable to an experimental verification. We perform an experimental test of the steering paradox in a two-qubit scenario. Furthermore, by starting from the steering paradox, we generate a generalized linear steering inequality and transform this inequality into a mathematically equivalent form, which is more friendly for experimental implementation, i.e., one may only measure the observables in x -, y -, or z -axis of the Bloch sphere, rather than other arbitrary directions. We also perform experiments to demonstrate this scheme. Within the experimental errors, the experimental results coincide with the theoretical predictions. Our results deepen the understanding of quantum foundations and provide an efficient way to detect the steerability of quantum states.

1. INTRODUCTION

Quantum paradox has provided an intuitive way to reveal the essential difference between quantum mechanics and classical theory. In 1935, by considering a continuous-variable entangled state $\Psi(x_1, x_2) = \int_{-\infty}^{+\infty} e^{ip(x_1-x_2+x_0)/\hbar} dp$, Einstein, Podolsky and Rosen (EPR) proposed a thought experiment to highlight a famous paradox [1]: either the quantum wavefunction does not provide a complete description of physical reality, or measuring one particle from a quantum entangled pair instantaneously affects the second particle regardless of how far apart the two entangled particles are. The EPR paradox has revealed a sharp conflict between local realism and quantum mechanics, thus triggering the investigation of nonlocal properties of quantum entangled states. Soon after the publication of the EPR paper, Schrödinger made an immediate response by introducing the term “steering” to depict “the spooky action at a distance” that was mentioned in the EPR argument [2]. According to Schrödinger, “steering” reflects a nonlocal phenomenon which, in a bipartite scenario, describes the ability of one party, say Alice, to prepare the other party (say Bob) particle in different quantum states by simply measuring her own particle using different settings. However, the notion of steering has not been gained much attention and development until 2007, when Wiseman *et al.* gave a rigorous definition using concepts from quantum information [3].

Undoubtedly, the EPR paradox is a milestone in quantum foundations, for it has opened the door of “quantum nonlocality”. In 1964, Bell made a distinct response to the EPR paradox by showing that quantum entangled states may vio-

late Bell inequality, which hold for any local-hidden-variable model [4]. This indicates that the local-hidden-variable models cannot reproduce all quantum predictions, and the violation of Bell inequality by entangled states directly implies that a kind of nonlocal properties – Bell nonlocality. Since then, Bell nonlocality has been achieved a rapid and fruitful development in two directions [5]: (i) On one hand, more and more Bell's inequalities have been introduced to detect Bell's nonlocality in different physical systems, for examples, the Clauser-Horne-Shimony-Holt (CHSH) inequality for two qubits [6], the Mermin-Ardehali-Belinskii-Klyshko (MABK) inequality for multipartite qubits [7], the Collins-Gisin-Linden-Masser-Popescu inequality for two qudits [8]. (ii) On the other hand, some novel quantum paradoxes, or the all-versus-nothing (AVN) proofs have been suggested to reveal Bell's nonlocality without inequalities. Typical examples are the Greenberger-Horne-Zeilinger (GHZ) paradox [9] and the Hardy paradox [10]. Experimental verifications of Bell nonlocality have also been carried out, for instances, Aspect *et al.* have successfully made the first observation of Bell's nonlocality with the CHSH inequality [11], Pan *et al.* have tested the three-qubit GHZ paradox in the photon-based experiment [12], and very recently Luo *et al.* have tested the generalized Hardy paradox for the multi-qubit systems [13].

Despite of being developed from the EPR paradox, Bell nonlocality does not directly correspond to the EPR paradox. As pointed out in Ref. [3], inspired by the EPR argument, one can derive three different types of “quantum nonlocality”: quantum entanglement, quantum steering, and Bell nonlocality. The original EPR paradox is actually a special case

of quantum steering [14]. Although quantum steering has been experimentally demonstrated in various quantum systems [15–24], all of these experiments just indirectly illustrate the EPR paradox, in which most of them are based on statistical inequalities. Here the direct illustration of a quantum paradox means that we can find a contradiction equality for this paradox and demonstrate it (the ref. [16] is a AVN proof but not a contradiction equality). For examples, (i) The GHZ paradox [9] can be formulated as a contradiction equality “+1 = -1”, where “+1” represents the prediction of the local-hidden-variable model, while “-1” is the quantum prediction. Thus, if one observes the value of “-1” by some quantum technologies in the experiments, then the GHZ paradox is demonstrated. (ii) The formulation of the Hardy paradox [10] is given as follows: under some certain Hardy-type constraints for probabilities $P_1 = P_2 = \dots = P_N = 0$, any local-hidden-variable model predicts a zero-probability (i.e., $P_{\text{succ}} = 0$), while quantum prediction is $P_{\text{succ}} > 0$, where P_{succ} is the success probability of a specific event. Upon successfully measuring the desired non-zero success probability under the required Hardy constraints, one verifies the Hardy paradox. A natural question arises whether the EPR paradox, which excludes any local-hidden-state (LHS) model, can be illustrated in a direct way just like GHZ or Hardy paradox?

The purpose of this paper is two-fold: (i) Based on our previous results of the steering paradox “2 = 1” [25], we present a generalized steering paradox “ $k = 1$ ”. We have also performed an experiment to illustrate the original EPR paradox through demonstrating the steering paradox “2 = 1” in a two-qubit scenario. (ii) A steering paradox can correspond to an inequality (e.g., the two-qubit Hardy paradox may correspond to the well-known CHSH inequality) [26, 27], and from the steering paradox “ $k = 1$ ”, we generate a generalized linear steering inequality (GLSI), which naturally includes the usual linear steering inequality as a special case [3, 15]. Besides, the GLSI can be transformed into a mathematically equivalent form, but is more friendly for experimental implementation, i.e., one may only measure the observables in x -, y -, or z -axis of the Bloch sphere, rather than other arbitrary directions. Meanwhile, we also experimentally test quantum violations of the GLSI, which shows that it is more powerful than the usual one in detecting the steerability of quantum states.

2. THE EPR PARADOX AS A STEERING PARADOX “ $k = 1$ ”

Following Ref.[25], let us consider an arbitrary two-qubit pure entangled state $\rho_{AB} = |\Psi(\alpha, \varphi)\rangle\langle\Psi(\alpha, \varphi)|$ shared by Alice and Bob. Using the Schmidt decomposition, i.e., in the \hat{z} -direction representation, the wave-function $|\Psi(\alpha, \varphi)\rangle$ may be written as

$$|\Psi(\alpha, \varphi)\rangle = \cos \alpha |00\rangle + e^{i\varphi} \sin \alpha |11\rangle, \quad (1)$$

with $\alpha \in (0, \pi/2)$, $\varphi \in [0, 2\pi]$. For the same state Eq. (1), in the general \hat{n} -direction decomposition one may recast it to

$$|\Psi(\alpha, \varphi)\rangle = |+\hat{n}\rangle|\chi_{+\hat{n}}\rangle + |-\hat{n}\rangle|\chi_{-\hat{n}}\rangle, \quad (2)$$

where $|\pm\hat{n}\rangle$ are the eigenstates of the operator $\hat{P}_a^{\hat{n}} = [\mathbb{1} + (-1)^a \vec{\sigma} \cdot \hat{n}]/2$ denoting Alice’s projective measurement on her qubit along the \hat{n} -direction with measurement outcomes a ($a = 0, 1$), $\mathbb{1}$ is the identity matrix, $\vec{\sigma} = (\sigma_x, \sigma_y, \sigma_z)$ is the vector of Pauli matrices, and $|\chi_{\pm\hat{n}}\rangle = \langle\pm\hat{n}|\Psi(\alpha, \varphi)\rangle$ are the collapsed pure states (unnormalized) for Bob’s qubit.

By performing a projective measurement on her qubit along the \hat{n} -direction, Alice, by wavefunction collapse, steers Bob’s qubit to the pure states $\rho_a^{\hat{n}} = \tilde{\rho}_a^{\hat{n}}/\text{tr}(\tilde{\rho}_a^{\hat{n}})$ with the probability $\text{tr}(\tilde{\rho}_a^{\hat{n}})$, here $\tilde{\rho}_a^{\hat{n}} = \text{tr}_A[(\hat{P}_a^{\hat{n}} \otimes \mathbb{1}) \rho_{AB}]$ are the so-called Bob’s unnormalized conditional states and $\rho_a^{\hat{n}}$ are the normalized ones [3]. In a two-setting steering protocol $\{\hat{z}, \hat{x}\}$, if Bob’s four unnormalized conditional states can be simulated by an ensemble $\{\wp_\xi \rho_\xi\}$ of the LHS model, then these may be described as [25]

$$\tilde{\rho}_0^{\hat{z}} = \cos^2 \alpha |0\rangle\langle 0| = \wp_1 \rho_1, \quad (3a)$$

$$\tilde{\rho}_1^{\hat{z}} = \sin^2 \alpha |1\rangle\langle 1| = \wp_2 \rho_2, \quad (3b)$$

$$\tilde{\rho}_0^{\hat{x}} = (1/2)|\chi_+\rangle\langle\chi_+| = \wp_3 \rho_3, \quad (3c)$$

$$\tilde{\rho}_1^{\hat{x}} = (1/2)|\chi_-\rangle\langle\chi_-| = \wp_4 \rho_4, \quad (3d)$$

where $|\chi_{\pm}\rangle = \cos \alpha |0\rangle \pm e^{i\varphi} \sin \alpha |1\rangle$ are normalized pure states, the ρ_i are hidden states, and the \wp_i represent the corresponding probabilities in the ensemble. They satisfy the constraint $\sum_\xi \wp_\xi \rho_\xi = \rho_B = \text{tr}_A[\rho_{AB}]$, where ρ_B is the reduced density matrix of Bob. On the other hand, since $\tilde{\rho}_0^{\hat{n}} + \tilde{\rho}_1^{\hat{n}} = \rho_B$ and $\text{tr} \rho_B = 1$, if we sum up terms in Eq. (3) and take the trace, we arrive at the contradiction “2 = 1”, which represents the EPR paradox in the two-setting steering protocol.

Here we show that a more general steering paradox “ $k = 1$ ” can be similarly obtained if one considers a k -setting steering scenario $\{\hat{n}_1, \hat{n}_2, \dots, \hat{n}_k\}$, in which Alice performs k projective measurements on her qubit along \hat{n}_j -directions (with $j = 1, 2, \dots, k$). For each projective measurement $\hat{P}_a^{\hat{n}_j}$, Bob obtains the corresponding unnormalized pure states $\tilde{\rho}_a^{\hat{n}_j}$. Suppose these states can be simulated by the LHS model, then one may obtain the following set of $2k$ equations:

$$\tilde{\rho}_0^{\hat{n}_j} = \sum_\xi \wp(0|\hat{n}_j, \xi) \wp_\xi \rho_\xi, \quad (4a)$$

$$\tilde{\rho}_1^{\hat{n}_j} = \sum_\xi \wp(1|\hat{n}_j, \xi) \wp_\xi \rho_\xi, \quad (j = 1, 2, \dots, k). \quad (4b)$$

Since the $\tilde{\rho}_a^{\hat{n}_j}$ ’s are proportional to pure states, the sum of the right-hand side of Eq. (4) actually contains only one ρ_ξ , as we have seen for Eq. (3). Furthermore, due to the relations $\tilde{\rho}_0^{\hat{n}_j} + \tilde{\rho}_1^{\hat{n}_j} = \rho_B$ and $\sum_{\xi=1}^{2k} \wp_\xi \rho_\xi = \rho_B$, and by taking trace of Eq. (4), one immediately has the steering paradox “ $k = 1$ ”.

Experimentally, we shall test the EPR paradox for a two-qubit system in the simplest case of $k = 2$. To this aim, we need to perform measurements leading to four quantum probabilities. The first one is $P_1^{\text{QM}} = \text{tr}[\tilde{\rho}_0^{\hat{z}} |0\rangle\langle 0|] = \cos^2 \alpha$, which is obtained from Bob by performing the projective measurement $|0\rangle\langle 0|$ on his unnormalized conditional state as in Eq. (3a). Similarly, from Eq. (3b)-Eq. (3d), one has $P_2^{\text{QM}} =$

$\text{tr}[\hat{\rho}_1^z |1\rangle\langle 1|] = \sin^2 \alpha$, $P_3^{\text{QM}} = \text{tr}[\hat{\rho}_0^x |\chi_+\rangle\langle \chi_+|] = 1/2$, and $P_4^{\text{QM}} = \text{tr}[\hat{\rho}_1^x |\chi_-\rangle\langle \chi_-|] = 1/2$. Consequently, the total quantum prediction is $P_{\text{total}}^{\text{QM}} = \sum_{i=1}^4 P_i^{\text{QM}} = 2$, which contradicts the LHS-model prediction “1”. If, within the experimental measurement errors, one obtains a value $P_{\text{total}}^{\text{QM}} \approx 2$, then the steering paradox “2 = 1” is demonstrated.

GENERALIZED LINEAR STEERING INEQUALITY

Just like Bell’s inequalities may be derived from the GHZ and Hardy paradoxes [26, 27], this is also the case for the EPR paradox. In turn, from the steering paradox “ $k = 1$ ”, one may derive a k -setting generalized linear steering inequality as follows: In the steering scenario $\{\hat{n}_1, \hat{n}_2, \dots, \hat{n}_k\}$, Alice performs k projective measurements along \hat{n}_j -directions. Upon preparing the two-qubit system in the pure state $|\Psi(\theta, \phi)\rangle$ (note that this is not $|\Psi(\alpha, \varphi)\rangle$ and here $|\Psi(\theta, \phi)\rangle$ is used to derive the inequality), for each measurement $\hat{P}_a^{\hat{n}_j}$, Bob has the corresponding normalized pure states as $\rho_a^{\hat{n}_j}(\theta, \phi) = \hat{\rho}_a^{\hat{n}_j} / \text{tr}(\hat{\rho}_a^{\hat{n}_j})$, where $\hat{\rho}_a^{\hat{n}_j} = \text{tr}_A[(\hat{P}_a^{\hat{n}_j} \otimes \mathbb{1}) |\Psi(\theta, \phi)\rangle\langle \Psi(\theta, \phi)|]$ with $(a = 0, 1)$. Then the k -setting GLSI is given by (see Appendix A)

$$S_k(\theta, \phi) = \sum_{j=1}^k \left(\sum_{a=0}^1 P(A_{n_j} = a) \langle \rho_a^{\hat{n}_j}(\theta, \phi) \rangle \right) \leq C_{\text{LHS}}, \quad (5)$$

which is a (θ, ϕ) -dependent inequality, where C_{LHS} is the classical bound determined by the maximal eigenvalue of $S_k(\theta, \phi)$ for the given values of θ and ϕ , $P(A_j = a)$ is the probability of the j -th measurement of Alice with outcome a , and $\rho_a^{\hat{n}_j}(\theta, \phi) = |\chi_{\pm}^j(\theta, \phi)\rangle\langle \chi_{\pm}^j(\theta, \phi)|$ corresponds to Bob’s projective measurements. This inequality can be used to detect the steerability of two-qubit pure or mixed states.

The GLSI has two remarkable advantages over the usual LSI [15]: (i) Based on its own form as in Eq. (5), the GLSI includes naturally the usual LSI as a special case, thus can detect more quantum states. In particular, the GLSI can detect the steerability for all pure entangled states Eq. (1) in the whole region $\alpha \in (0, \pi/2)$, at variance with the usual LSI, which fails to detect EPR steering for some regions of α close to 0 [28]. (ii) The use of GLSI reduces the numbers of experimental measurements and improves the experimental accuracy. This may be seen as follow: with the usual k -setting LSI, Bob needs to perform k measurements in different k directions, for different input states ρ_{AB} . This is experimentally challenging since it may be hard to suitably tune the setup for all the k directions. However, with the GLSI one may solve this issue using the Bloch realization $|\chi_{\pm}^j\rangle\langle \chi_{\pm}^j| = (\mathbb{1} + \vec{\sigma} \cdot \hat{n}_{\pm}^j)/2$, which transforms the GLSI to an equivalent form where Bob only needs to perform measurements along the \hat{x} , \hat{y} and \hat{z} directions of the Bloch sphere, which are independent on the input states (see Appendix A).

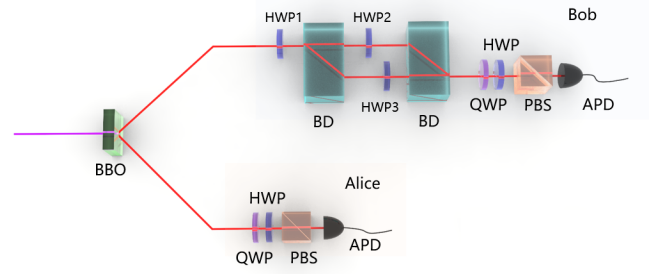


FIG. 1: **Experimental setup.** Polarization-entangled photons pairs are generated via nonlinear crystal. An asymmetric loss interferometer along with half-wave plates (HWPs) are used to prepare two-qubit pure entangled states. The projective measurements are performed using wave plates and polarization beam splitter (PBS).

To be more specific, we give an example of the 3-setting GLSI from Eq. (5), where Alice’s three measuring directions are $\{\hat{x}, \hat{y}, \hat{z}\}$. Then we immediately have

$$S_3 = P(A_x = 0) \langle |\chi_+\rangle\langle \chi_+| \rangle + P(A_x = 1) \langle |\chi_-\rangle\langle \chi_-| \rangle + P(A_y = 0) \langle |\chi'_+\rangle\langle \chi'_+| \rangle + P(A_y = 1) \langle |\chi'_-\rangle\langle \chi'_-| \rangle + P(A_z = 0) \langle |0\rangle\langle 0| \rangle + P(A_z = 1) \langle |1\rangle\langle 1| \rangle \leq C_{\text{LHS}}, \quad (7)$$

with $|\chi_{\pm}\rangle = \cos \theta |0\rangle \pm e^{i\phi} \sin \theta |1\rangle$, $|\chi'_{\pm}\rangle = \cos \theta |0\rangle \mp ie^{i\phi} \sin \theta |1\rangle$, $C_{\text{LHS}} = \text{Max}\{\frac{3+C_+}{2}, \frac{3+C_-}{2}\}$, and $C_{\pm} = \sqrt{4 \pm 4 \cos 2\theta + \cos 4\theta}$. The equivalent 3-setting steering inequality is given by (see Appendix B)

$$S'_3(\theta, \phi) = \sin 2\theta \cos \phi \langle A_x \sigma_x \rangle - \sin 2\theta \cos \phi \langle A_y \sigma_y \rangle + \sin 2\theta \sin \phi \langle A_x \sigma_y \rangle + \sin 2\theta \sin \phi \langle A_y \sigma_x \rangle + \langle A_z \sigma_z \rangle + 2 \cos 2\theta \langle \sigma_z \rangle \leq C'_{\text{LHS}}, \quad (8)$$

with $C'_{\text{LHS}} = \text{Max}\{C_+, C_-\}$. Obviously, by taking $\theta = \pi/4, \phi = 0$, the inequality Eq. (8) reduces to the usual 3-setting LSI in the form [15]:

$$S'_3(\pi/4, 0) = \langle A_x \sigma_x \rangle - \langle A_y \sigma_y \rangle + \langle A_z \sigma_z \rangle \leq \sqrt{3}. \quad (9)$$

In the experiment to test the inequalities, Alice prepares two qubits and sends one of them to Bob, who trusts his own measurements but not Alice’s. Bob asks Alice to measure at random σ_x, σ_y or σ_z on her qubit with or simply not to perform any measurement; then Bob measures σ_x, σ_y or σ_z on his qubit with according to Alice’s measurement. Finally, Bob evaluates the average values $\langle \sigma_x \otimes \sigma_x \rangle, \langle \sigma_y \otimes \sigma_y \rangle, \langle \sigma_x \otimes \sigma_y \rangle, \langle \sigma_y \otimes \sigma_x \rangle, \langle \sigma_z \otimes \sigma_z \rangle$, and $\langle \mathbb{1} \otimes \sigma_z \rangle$ and is therefore capable of checking whether the steering inequality Eq. (8) is violated or not. In particular, for the case of pure states Eq. (1), if Alice is honest in the preparation and measurements of the states, the inequalities are violated for all values of α and φ (except at $\alpha = 0, \pi/2$), thereby confirming Alice’s ability to steer Bob.

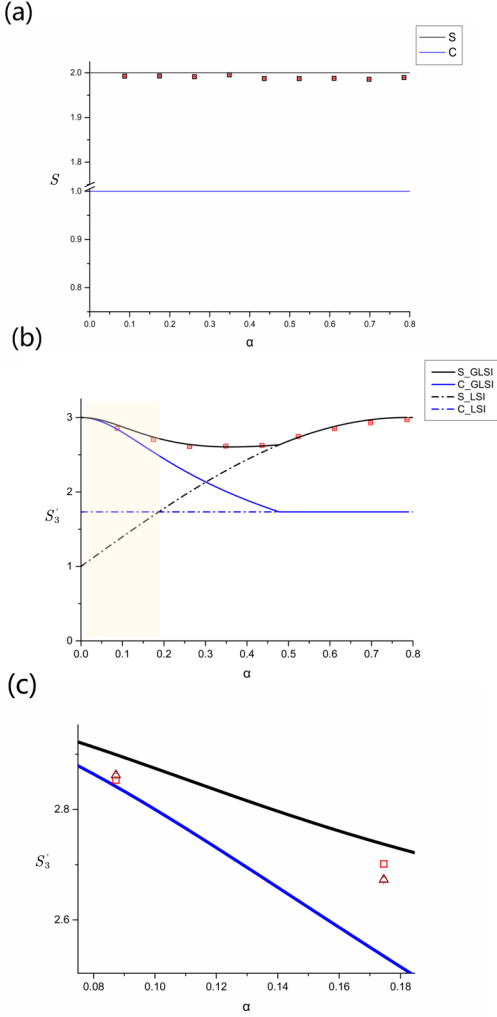


FIG. 2: **Experimental results for pure states.** In panel (a) we show the experimental results concerning the steering paradox “2=1”. The black and blue solid lines represent the quantum prediction $S \equiv P_{\text{total}}^{\text{QM}} = 2$ and the classical bound $C = 1$ based on the LHV models, respectively. The black cubes and the red lines show the experimental results with error bar. Panel (b) shows the experimental results for the 3-setting GLSI of Eq. (8). The black and blue solid line represent the quantum and classic bound, respectively, which are obtained by maximizing the difference between S'_3 and C'_{LHS} for any fixed α . The black (blue) dot line represents the quantum violations $\langle S'_3 \rangle = 1 + 2 \sin(2\alpha)$ (the classical value $C = \sqrt{3}$) of the usual 3-setting LSI Eq. (9), respectively. The red cubes are the experimental points for the inequality Eq. (8). The light yellow range is $\alpha \in (0, (\arcsin(\frac{\sqrt{3}-1}{2}))/2]$, where the LSI Eq. (9) cannot detect the steerability but the GLSI can. Panel (c) shows the experimental violation for $\alpha = \frac{\pi}{36}, \frac{\pi}{18}$.

3. EXPERIMENTAL RESULTS

The experimental setup is shown in Fig. 1, the degenerated polarization-entangled photon pairs are created by spontaneous parametric down-conversion [29] type-II barium bo-

rate (BBO) crystal pumped by a 404nm laser. The initial two-photon state is singlet state $|\psi\rangle = (|HV\rangle - |VH\rangle)/\sqrt{2}$. By setting HWP1 at 0° (correspond to a phase gate) one may switch the phase of entangled state from “minus” to “plus”. HWP2, HWP3 and beam displacers (BD) are used to construct an asymmetric loss interferometer to adjust the amplitude and flip the qubit, where HWP3 fixed at 45° and HWP2 at $\arcsin(\sqrt{\frac{1}{\sin^2 \alpha} - 1}) \cdot \frac{90}{\pi} \in [0, 45^\circ]$. Therefore, we may prepare desired two-qubit state as $|\Psi(\alpha)\rangle = \cos \alpha |HH\rangle + \sin \alpha |VV\rangle$ (see Appendix C). Now we define $|H\rangle = |0\rangle$ and $|V\rangle = |1\rangle$, the entangled state becomes $|\Psi(\alpha)\rangle = \cos \alpha |00\rangle + \sin \alpha |11\rangle$. Compare with Eq. (1), in our experiment, the phase φ of the entangled state is set to 0. As illustrated in Fig. 1, after preparation of entangled state, we sent the first qubit to Alice, and the second to Bob. Then Alice and Bob measure their own photons through the polarization analyzer, which consists of quarter-wave plate (QWP), HWP and PBS, and test EPR steering.

First, we test the EPR paradox via steering paradox “2 = 1” by choosing α from $\frac{\pi}{36}$ to $\frac{\pi}{4}$ with an interval of $\frac{\pi}{36}$ to obtain nine different two-qubit entangled states. In the two-setting steering scenario, Alice performs measurements on her photon along the \hat{x} -direction and \hat{z} -direction of Bloch sphere. The eigenvectors of σ_x are $|\pm\rangle = (|0\rangle \pm |1\rangle)/\sqrt{2}$, which are the states on which the photon of Alice may collapse with a certain probability. The corresponding normalized conditional states for Bob are given by $|\chi_{\pm}\rangle = \cos \alpha |0\rangle \pm \sin \alpha |1\rangle$. Similarly, Bob’s normalized conditional states are $|0\rangle$ and $|1\rangle$ when Alice performs corresponding measurements. As shown in Fig. 2(a), the experimental values $S = P_{\text{total}}^{\text{Q}}$ for the nine different entangled pure states largely exceed the classical prediction. The average value is $S \approx 1.9899$, which is far exceeds above the classical bound predicted by LHS models. Thus, the steering paradox has been successfully demonstrated.

Second, we experimentally address the violations of the GLSI using above pure states $|\Psi(\alpha)\rangle$. We experimentally evaluate the value of S'_3 by using the 3-setting steering inequality Eq. (8). For simplicity, in our experiment the phase ϕ is set to 0, and therefore, following Eq. (8), we only need to measure the following four expectation values: $\langle \sigma_x \otimes \sigma_x \rangle$, $\langle \sigma_y \otimes \sigma_y \rangle$, $\langle \sigma_z \otimes \sigma_z \rangle$, and $\langle \sigma_I \otimes \sigma_z \rangle$. Besides, in order to experimentally observe the violation of the GLSI for any $\alpha \in (0, \pi/4]$, we have to maximize the difference between S'_3 and classical bound C'_{LHS} at any fixed value α . This is done by numerically solving the optimal solutions of θ . Remarkably, for $\alpha \in (0, (\arcsin(\frac{\sqrt{3}-1}{2}))/2 \approx \frac{\pi}{17}]$, one observes a significant violation of the inequality, which does not occur for the usual 3-setting LSI Eq. (9). On the other hand, when α is close to $\pi/4$, the violation of the GLSI Eq. (8) and the LSI Eq. (9) are of the same order. The experimental results are shown in Fig. 2(b) and (c), which are almost indistinguishable from the theoretical predictions.

Finally, we have experimentally tested inequality Eq. (8) with two types of mixed states (see Appendix C). The first

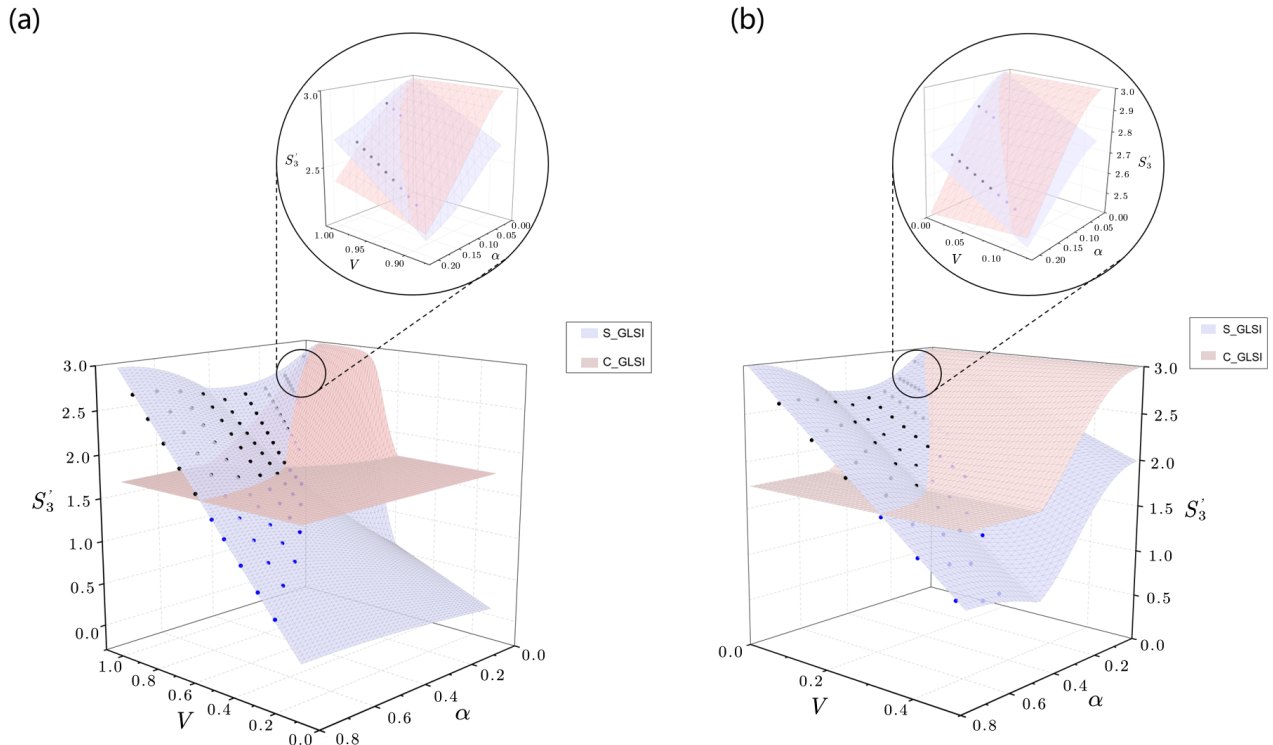


FIG. 3: **Experimental results for mixed states.** Panels (a) and (b) show the steering detection for the generalized Werner state ρ_1 and the asymmetric mixed state ρ_2 . The light purple and pink surfaces represent the quantum value and the classical bound of the GLSI (8), respectively. The black (blue) dots denote results for the quantum states that can (cannot) experimentally violate the GLSI (8). The zoom shows the area where steering cannot be detected by usual LSI (9), whereas GLSI may be useful.

one is a generalized Werner state ρ_1 [30] and the second one is the asymmetric mixed state ρ_2 [31], which are given as

$$\rho_1 = V|\Psi(\alpha)\rangle\langle\Psi(\alpha)| + \frac{1-V}{4}\mathbb{1} \otimes \mathbb{1}, \quad (10a)$$

$$\rho_2 = V|\Psi(\alpha)\rangle\langle\Psi(\alpha)| + (1-V)|\Phi(\alpha)\rangle\langle\Phi(\alpha)|, \quad (10b)$$

with $|\Phi(\alpha)\rangle = \sin\alpha|01\rangle + \cos\alpha|10\rangle$, $\alpha \in [0, \frac{\pi}{4}]$, and $V \in [0, 1]$. As it is apparent from Fig. 3(a) and Fig. 3(b), the experimental results confirm that the GLSI has an advantage over the LSI in detecting steerability for more quantum states (One can see Appendix B for more theoretical details).

4. CONCLUSIONS

In summary, we have advanced the study of EPR paradox in two aspects: (i) We have presented a generalized steering paradox “ $k = 1$ ” and performed an experiment to illustrate the original EPR paradox through demonstrating the steering paradox “ $2 = 1$ ” in a two-qubit scenario. (ii) Based on the steering paradox “ $k = 1$ ”, we have successfully generated a k -setting generalized linear steering inequality, which may detect steerability of quantum states to a larger extent than the previous ones. We have also rewritten this inequality into a mathematically equivalent form, which is more suitable for

experimental implementation since it allows us to measure only along the x -, y -, or z -axis in Bloch sphere, rather than other arbitrary directions, and thus greatly simplifying the experimental setups and improving precision. This finding is valuable for the open problem of how to optimize the measurement settings for steering verification in experiments [32]. Our results deepen the understanding of quantum foundations and provide an efficient way to detect the steerability of quantum states.

Recently, quantum steering has been applied to the one-side device-independent quantum key distribution protocol to secure shared keys by measuring the quantum steering inequality [33]. Our generalized linear steering inequality can also be applied to this scenario to implement the one-side DIQKD. In addition, our results may be applied to applications such as quantum random number generation [34, 35] and quantum sub-channel discrimination [36, 37].

APPENDIX A. GENERALIZED LINEAR STEERING INEQUALITY OBTAINED FROM THE GENERAL STEERING PARADOX “ $k = 1$ ”.

Actually, from the steering paradox “ $k = 1$ ”, one can naturally derive a k -setting generalized linear steering inequality

(GLSI), which include the usual LSI [15] as special case.

The derivation procedure is as follows: In the steering scenario $\{\hat{n}_1, \hat{n}_2, \dots, \hat{n}_k\}$, Alice performs k projective measurements $\hat{P}_a^{\hat{n}_j}$. For the pure state $|\Psi(\theta, \phi)\rangle$ as shown in Eq. (1), it can have an equivalent but more general decomposition along the \hat{n} -direction as Eq. (2). Explicitly, Alice's projective measurements could be rewritten as

$$\hat{P}_0^{\hat{n}_j} = \frac{\mathbb{1} + \hat{n}_j \cdot \vec{\sigma}}{2} = |+\hat{n}\rangle\langle+\hat{n}|, \quad (11a)$$

$$\hat{P}_1^{\hat{n}_j} = \frac{\mathbb{1} - \hat{n}_j \cdot \vec{\sigma}}{2} = |-\hat{n}\rangle\langle-\hat{n}|. \quad (11b)$$

Based on the two-qubit pure state $|\Psi(\theta, \phi)\rangle$, for the j -th projective measurement $\hat{P}_a^{\hat{n}_j}$ of Alice, Bob will have the unnormalized conditional states as

$$\tilde{\rho}_0^{\hat{n}_j} = \text{tr}_A[(\hat{P}_0^{\hat{n}_j} \otimes \mathbb{1}) |\Psi\rangle\langle\Psi|] = |\chi_{+\hat{n}_j}\rangle\langle\chi_{+\hat{n}_j}|, \quad (12a)$$

$$\tilde{\rho}_1^{\hat{n}_j} = \text{tr}_A[(\hat{P}_1^{\hat{n}_j} \otimes \mathbb{1}) |\Psi\rangle\langle\Psi|] = |\chi_{-\hat{n}_j}\rangle\langle\chi_{-\hat{n}_j}|, \quad (12b)$$

and from which one has the normalized conditional states as

$$\rho_0^{\hat{n}_j} = \frac{\tilde{\rho}_0^{\hat{n}_j}}{\text{tr}(\tilde{\rho}_0^{\hat{n}_j})} = |\chi_+^j\rangle\langle\chi_+^j|, \quad (13a)$$

$$\rho_1^{\hat{n}_j} = \frac{\tilde{\rho}_1^{\hat{n}_j}}{\text{tr}(\tilde{\rho}_1^{\hat{n}_j})} = |\chi_-^j\rangle\langle\chi_-^j|, \quad (13b)$$

with

$$|\chi_+^j\rangle = \frac{|\chi_{+\hat{n}_j}\rangle}{\sqrt{\text{tr}[|\chi_{+\hat{n}_j}\rangle\langle\chi_{+\hat{n}_j}|]}}, \quad (14)$$

$$|\chi_-^j\rangle = \frac{|\chi_{-\hat{n}_j}\rangle}{\sqrt{\text{tr}[|\chi_{-\hat{n}_j}\rangle\langle\chi_{-\hat{n}_j}|]}}, \quad (15)$$

are pure states. Obviously, for the pure state $|\Psi\rangle$, the following probability relation is always hold:

$$\text{tr}[(\hat{P}_0^{\hat{n}_j} \otimes |\chi_+^j\rangle\langle\chi_+^j|) |\Psi\rangle\langle\Psi|] + \quad (16)$$

$$\text{tr}[(\hat{P}_1^{\hat{n}_j} \otimes |\chi_-^j\rangle\langle\chi_-^j|) |\Psi\rangle\langle\Psi|] = \quad (17)$$

$$\text{tr}[|\chi_{+\hat{n}_j}\rangle\langle\chi_{+\hat{n}_j}|] + \text{tr}[|\chi_{-\hat{n}_j}\rangle\langle\chi_{-\hat{n}_j}|] \equiv 1. \quad (18)$$

The quantity in the left-hand-side of Eq. (16) can be used to construct the steering inequality, where for the Alice's side we need to replace the quantum measurement operator $\hat{P}_a^{\hat{n}_j}$ by their correspondingly classical probabilities $P(A_{n_j} = a)$. Then we immediately have the k -setting GLSI as

$$\mathcal{S}_k = \sum_{j=1}^k \left(\sum_{a=0}^1 P(A_{n_j} = a) \langle \rho_a^{\hat{n}_j} \rangle \right) \leq C_{\text{LHS}}, \quad (19)$$

where $P(A_j = a)$ is the classical probability of the j -th measurement of Alice with outcome a ,

$$\rho_0^{\hat{n}_j} = |\chi_+^j\rangle\langle\chi_+^j|, \quad \rho_1^{\hat{n}_j} = |\chi_-^j\rangle\langle\chi_-^j|, \quad (20)$$

denote the projective measurements in Bob's side, C_{LHS} is the classical bound that determined by the maximal eigenvalue of

the steering parameter \mathcal{S}_k . By definition, it is easy to verify directly that for the pure state (1) the quantum prediction of \mathcal{S}_k is equal to k .

Remark 1.—In Ref. [15], the usual k -setting linear steering inequality is given as

$$\mathcal{S}_k^{\text{LSI}} = \sum_{j=1}^k A_j \langle \hat{m}_j \cdot \vec{\sigma} \rangle \leq C_{\text{LHS}}^{\text{LSI}}, \quad (21)$$

here $C_{\text{LHS}}^{\text{LSI}}$ denotes the classical bound for the LSI. Note that for the LSI Eq. (21), quantum mechanically Alice will perform k measurements (corresponds to $\hat{A}_j = \hat{n}_j \cdot \vec{\sigma}$), and Bob will also perform k measurements (corresponds to $\hat{B}_j = \hat{m}_j \cdot \vec{\sigma}$). In the following we would like to show that the LSI is a special case of the GLSI as given in Eq. (19).

Let us rewrite the projective measurements Eq. (20) in the Bloch-representation as

$$\begin{aligned} \rho_0^{\hat{n}_j} &= |\chi_+^j\rangle\langle\chi_+^j| = \frac{1}{2}(\mathbb{1} + \hat{m}_+^j \cdot \vec{\sigma}), \\ \rho_1^{\hat{n}_j} &= |\chi_-^j\rangle\langle\chi_-^j| = \frac{1}{2}(\mathbb{1} + \hat{m}_-^j \cdot \vec{\sigma}), \end{aligned} \quad (22)$$

and we denote

$$P(A_j = 0) = \frac{1 + A_j}{2}, \quad P(A_j = 1) = \frac{1 - A_j}{2}, \quad (23)$$

then by substituting Eqs. (22) and (23) into the inequality Eq. (19), we have

$$\begin{aligned} \mathcal{S}_k &= \sum_{j=1}^k \left(\frac{1 + A_j}{2} \langle \frac{1}{2}(\mathbb{1} + \hat{m}_+^j \cdot \vec{\sigma}) \rangle + \right. \\ &\quad \left. \frac{1 - A_j}{2} \langle \frac{1}{2}(\mathbb{1} + \hat{m}_-^j \cdot \vec{\sigma}) \rangle \right) \leq C_{\text{LHS}}. \end{aligned} \quad (24)$$

Note that for the GLSI Eq. (24), quantum mechanically Alice will perform k measurements (corresponds to $\hat{A}_j = \hat{n}_j \cdot \vec{\sigma}$), and Bob will perform $2k$ measurements (corresponds to $\hat{B}_j^+ = \hat{m}_+^j \cdot \vec{\sigma}$ and $\hat{B}_j^- = \hat{m}_-^j \cdot \vec{\sigma}$, if $\hat{m}_+^j \neq \pm \hat{m}_-^j$). In the following we would like to show that the LSI is a special case of the GLSI as given in Eq. (19).

Let

$$\hat{n}_j = (\sin \tau \cos \gamma, \sin \tau \sin \gamma, \cos \tau), \quad (26)$$

then

$$|+\hat{n}_j\rangle = \begin{pmatrix} \cos \frac{\tau}{2} \\ \sin \frac{\tau}{2} e^{i\gamma} \end{pmatrix}, \quad |-\hat{n}_j\rangle = \begin{pmatrix} \sin \frac{\tau}{2} \\ -\cos \frac{\tau}{2} e^{i\gamma} \end{pmatrix}, \quad (27)$$

which are eigenstates of $\hat{n}_j \cdot \vec{\sigma}$. From Eq. (2), one can explicitly have

$$|\chi_{+\hat{n}_j}\rangle = \langle +\hat{n}_j | \Psi(\theta, \phi) \rangle \quad (28)$$

$$= \cos \frac{\tau}{2} \cos \theta |0\rangle + e^{i(\phi-\gamma)} \sin \frac{\tau}{2} \sin \theta |1\rangle,$$

$$|\chi_{-\hat{n}_j}\rangle = \langle -\hat{n}_j | \Psi(\theta, \phi) \rangle \quad (29)$$

$$= \sin \frac{\tau}{2} \cos \theta |0\rangle - e^{i(\phi-\gamma)} \cos \frac{\tau}{2} \sin \theta |1\rangle, \quad (30)$$

which yields

$$\langle \chi_{-\hat{n}_j} | \chi_{+\hat{n}_j} \rangle = \cos \frac{\tau}{2} \sin \frac{\tau}{2} (\cos^2 \theta - \sin^2 \theta). \quad (31)$$

Namely, if $\theta = \pi/4$, the states $|\chi_{+\hat{n}_j}\rangle$ and $|\chi_{-\hat{n}_j}\rangle$ are orthogonal, then from Eq. (22) one immediately knows that the two Bloch vectors are antiparallel, i.e.,

$$\hat{m}_+^j = -\hat{m}_-^j \equiv \hat{m}^j. \quad (32)$$

Substituting the relation Eq. (32) into the inequality Eq. (24), we have

$$\mathcal{S}_k = \frac{1}{2} \sum_{j=1}^k \left(1 + A_j \langle \hat{m}^j \cdot \vec{\sigma} \rangle \right) \leq C_{\text{LHS}}$$

i.e.,

$$\mathcal{S}_k^{\text{LSI}} = \sum_{j=1}^k A_j \langle \hat{m}_j \cdot \vec{\sigma} \rangle \leq 2 C_{\text{LHS}} - k. \quad (33)$$

proving the usual LSI is a special case of the GLSI. In short, for an arbitrary two-qubit pure entangled state $|\Psi(\theta, \phi)\rangle$, one can have a steering paradox “ $k = 1$ ” [25], based on which one can derive a general linear steering inequality as shown in Eq. (19). If one further fixes the parameter θ as $\theta = \pi/4$ (in this case $|\Psi(\theta = \pi/4, \phi)\rangle$ is the maximally entangled state), then the GLSI reduces to the usual LSI.

Remark 2.—We may rewrite the GLSI Eq. (24) in a mathematically equivalent form, but which is more friendly for experimental implements. Let us denote

$$\hat{m}_+^j = (m_{+x}^j, m_{+y}^j, m_{+z}^j), \quad \hat{m}_-^j = (m_{-x}^j, m_{-y}^j, m_{-z}^j), \quad (34)$$

then from the inequality Eq. (24) one has

$$\begin{aligned} \mathcal{S}_k &= \sum_{j=1}^k \left(\frac{1+A_j}{2} \langle \frac{1}{2}(\mathbb{1} + \hat{m}_+^j \cdot \vec{\sigma}) \rangle + \frac{1-A_j}{2} \langle \frac{1}{2}(\mathbb{1} + \hat{m}_-^j \cdot \vec{\sigma}) \rangle \right) \\ &= \sum_{j=1}^k \left(\frac{1}{2} + \frac{1+A_j}{4} (\hat{m}_{+x}^j \langle \vec{\sigma}_x \rangle + \hat{m}_{+y}^j \langle \vec{\sigma}_y \rangle + \hat{m}_{+z}^j \langle \vec{\sigma}_z \rangle) + \frac{1-A_j}{4} (\hat{m}_{-x}^j \langle \vec{\sigma}_x \rangle + \hat{m}_{-y}^j \langle \vec{\sigma}_y \rangle + \hat{m}_{-z}^j \langle \vec{\sigma}_z \rangle) \right) \\ &\leq C_{\text{LHS}}. \end{aligned} \quad (35)$$

The remarkable point for the inequality Eq. (35) is that Bob always measures his particle in three directions of x, y, z , which not only greatly reduces the numbers of measurements and but also need not tune the measurement direction to other directions.

APPENDIX B. EPR STEERING BY USING THE 3-SETTING GENERALIZED LSI.

In this experimental work, we shall demonstrate EPR steering for the two-qubit generalized Werner state by using the generalized linear steering inequality. We focus on the 3-setting GLSI. In the steering scenario $\{\hat{x}, \hat{y}, \hat{z}\}$, Alice performs projective measurements on her qubit along the \hat{x} -, \hat{y} - and \hat{z} -directions, from Eq. (19) one immediately has

$$\begin{aligned} \mathcal{S}_3 &= P(A_x = 0) \langle |\chi_+\rangle \langle \chi_+| \rangle + P(A_x = 1) \langle |\chi_-\rangle \langle \chi_-| \rangle \\ &\quad + P(A_y = 0) \langle |\chi'_+\rangle \langle \chi'_+| \rangle + P(A_y = 1) \langle |\chi'_-\rangle \langle \chi'_-| \rangle \\ &\quad + P(A_z = 0) \langle |0\rangle \langle 0| \rangle + P(A_z = 1) \langle |1\rangle \langle 1| \rangle \\ &\leq C_{\text{LHS}}, \end{aligned} \quad (36)$$

with

$$\begin{aligned} |\chi_{\pm}\rangle &= \cos \theta |0\rangle \pm e^{i\phi} \sin \theta |1\rangle, \\ |\chi'_{\pm}\rangle &= \cos \theta |0\rangle \mp i e^{i\phi} \sin \theta |1\rangle. \end{aligned} \quad (37)$$

One can have

$$\begin{aligned} |\chi_+\rangle \langle \chi_+| &= \frac{1}{2}(\mathbb{1} + \hat{m}_+ \cdot \vec{\sigma}), & |\chi_-\rangle \langle \chi_-| &= \frac{1}{2}(\mathbb{1} + \hat{m}_- \cdot \vec{\sigma}), \\ |\chi'_+\rangle \langle \chi'_+| &= \frac{1}{2}(\mathbb{1} + \hat{m}'_+ \cdot \vec{\sigma}), & |\chi'_-\rangle \langle \chi'_-| &= \frac{1}{2}(\mathbb{1} + \hat{m}'_- \cdot \vec{\sigma}), \\ |0\rangle \langle 0| &= \frac{1}{2}(\mathbb{1} + \sigma_z), & |1\rangle \langle 1| &= \frac{1}{2}(\mathbb{1} - \sigma_z), \end{aligned} \quad (38)$$

with

$$\begin{aligned} \hat{m}_+ &= (\sin 2\theta \cos \phi, \sin 2\theta \sin \phi, \cos 2\theta), \\ \hat{m}_- &= (-\sin 2\theta \cos \phi, -\sin 2\theta \sin \phi, \cos 2\theta), \\ \hat{m}'_+ &= (\sin 2\theta \sin \phi, -\sin 2\theta \cos \phi, \cos 2\theta), \\ \hat{m}'_- &= (-\sin 2\theta \sin \phi, \sin 2\theta \cos \phi, \cos 2\theta). \end{aligned} \quad (39)$$

We now come to compute the the classical bound C_{LHS} . Because $P(A_i = 0) + P(A_i = 1) = 1$, ($i = x, y, z$), i.e.,

$P(A_i = 0)$ is exclusive with $P(A_i = 1)$, if $P(A_i = 0) = 1$, then one must have $P(A_i = 1) = 0$. For the inequality (Eq. 36), there are totally eight combinations:

(i) $P(A_z = 0) = P(A_x = 0) = P(A_y = 0) = 1$, then the left-hand side of the inequality Eq. (36) is

$$\left\langle |\chi_+\rangle\langle\chi_+| + |\chi'_+\rangle\langle\chi'_+| + |0\rangle\langle 0| \right\rangle, \quad (40)$$

for such matrix, its two eigenvalues are

$$\frac{3 + \sqrt{4 - 4 \cos 2\theta + \cos 4\theta}}{2}, \quad (41)$$

$$\frac{3 - \sqrt{4 - 4 \cos 2\theta + \cos 4\theta}}{2}. \quad (42)$$

Similarly, for $P(A_z = 0) = P(A_x = 0) = P(A_y = 1) = 1$, $P(A_z = 0) = P(A_x = 1) = P(A_y = 0) = 1$, $P(A_z = 0) = P(A_x = 1) = P(A_y = 1) = 1$.

(ii) $P(A_z = 1) = P(A_x = 0) = P(A_y = 0) = 1$, then the left-hand side of the inequality Eq. (36) is

$$\left\langle |\chi_+\rangle\langle\chi_+| + |\chi'_+\rangle\langle\chi'_+| + |1\rangle\langle 1| \right\rangle, \quad (43)$$

for such matrix, its two eigenvalues are

$$\frac{3 + \sqrt{4 + 4 \cos 2\theta + \cos 4\theta}}{2}, \quad (44)$$

$$\frac{3 - \sqrt{4 + 4 \cos 2\theta + \cos 4\theta}}{2}. \quad (45)$$

Similarly, for $P(A_z = 1) = P(A_x = 0) = P(A_y = 1) = 1$, $P(A_z = 1) = P(A_x = 1) = P(A_y = 0) = 1$, $P(A_z = 1) = P(A_x = 1) = P(A_y = 1) = 1$.

Thus, in summary, the classical bound is given by (here $\theta \in (0, \pi/2)$)

$$C_{\text{LHS}} = \text{Max}\left\{ \frac{3 + C_+}{2}, \frac{3 + C_-}{2} \right\}, \quad (46)$$

with

$$C_{\pm} = \sqrt{4 \pm 4 \cos 2\theta + \cos 4\theta}. \quad (47)$$

Obviously the classical bound $C_{\text{LHS}} \leq 3$, however, for any two-qubit pure entangled state $|\Psi(\theta, \phi)\rangle$ one has $\mathcal{S}_3^{QM} = 3$, thus any two-qubit pure entangled state violates the steering inequality Eq. (36).

Let

$$P(A_i = 0) = \frac{1 + A_i}{2}, \quad P(A_i = 1) = \frac{1 - A_i}{2}, \quad (48)$$

where ($i = x, y, z$). Substituting Eqs. (38), (39) and (48) into the inequality Eq. (36) and after simplify, one obtains the equivalent 3-setting steering inequality as

$$\begin{aligned} \mathcal{S}'_3 &= \sin 2\theta \cos \phi \langle A_x \sigma_x \rangle - \sin 2\theta \cos \phi \langle A_y \sigma_y \rangle \\ &+ \sin 2\theta \sin \phi \langle A_x \sigma_y \rangle + \sin 2\theta \sin \phi \langle A_y \sigma_x \rangle \\ &+ \langle A_z \sigma_z \rangle + 2 \cos 2\theta \langle \sigma_z \rangle \leq C'_{\text{LHS}}, \end{aligned} \quad (49)$$

with $C'_{\text{LHS}} = \text{Max}\{C_+, C_-\}$. Obviously, by taking $\theta = \pi/4, \phi = 0$, the inequality Eq. (49) reduces to the usual 3-setting LSI (an equivalent form) in [15].

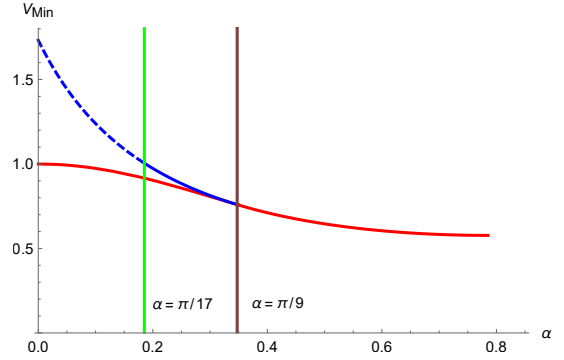


FIG. 4: Detecting EPR steerability of the generalized Werner state by using the usual 3-setting LSI (Blue line) and the 3-setting GLSI (Red line). For a fixed parameter α , the threshold value of the visibility is given by V_{min} , below which the steering inequalities cannot be violated. It can be observed that the GLSI is stronger than the usual LSI in detecting the EPR steerability.

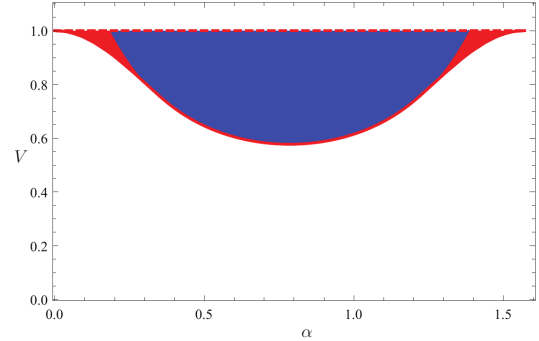


FIG. 5: The generalized Werner states violate the usual 3-setting LSI in the blue region, and violate the 3-setting generalized LSI in the red region. It can be observed that the GLSI is stronger than the usual LSI in detecting the EPR steerability.

Example 1.— Let us consider the two-qubit pure state $|\Psi(\alpha)\rangle = \cos \alpha |00\rangle + \sin \alpha |11\rangle$, its maximal violation value for the usual 3-setting steering inequality Eq. (9) is $1 + 2 \sin 2\alpha$. Hence, only when $\alpha > \frac{\arcsin \frac{\sqrt{3}-1}{2}}{2} \approx 0.1873$, the usual linear steering inequality can be violated. However, the pure state violates the GLSI Eq. (36) for the whole region $\alpha \in (0, \pi/2)$, thus the generalized LSI is stronger than the usual LSI in detecting the EPR steerability of pure entangled states.

Example 2.— Let us consider the two-qubit generalized Werner state

$$\rho_1 = \rho_{AB}(\alpha, V) = V |\Psi(\alpha)\rangle\langle\Psi(\alpha)| + \frac{1-V}{4} \mathbf{1} \otimes \mathbf{1}, \quad (50)$$

with $\alpha \in [0, \frac{\pi}{4}]$, $V \in [0, 1]$.

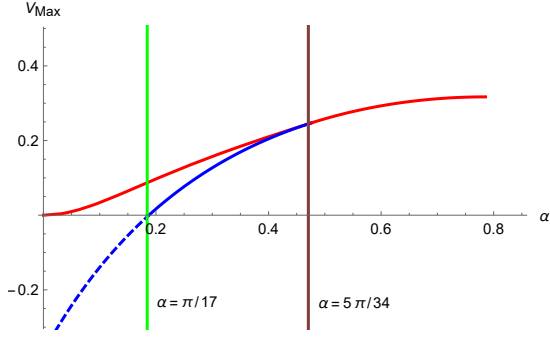


FIG. 6: Detecting EPR steerability of the mixed state Eq. (51) by using the usual 3-setting LSI (Blue line) and the 3-setting GLSI (Red line). For a fixed parameter α , the threshold value of the visibility is given by V_{\max} , above which the steering inequalities cannot be violated. It can be observed that the GLSI is stronger than the usual LSI in detecting the EPR steerability.

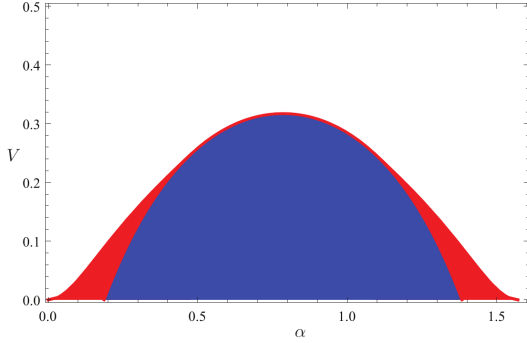


FIG. 7: The mixed states Eq. (51) violate the usual 3-setting LSI in the blue region, and violate the 3-setting GLSI in the red region. It can be observed that the GLSI is stronger than the usual LSI in detecting the EPR steerability.

For the state Eq. (50), we come to compare the performance between the usual 3-setting LSI (Blue line) and the 3-setting GLSI (Red line) in Fig. 4. For the usual LSI, the threshold value of the visibility is given by $V_{\min} = \frac{\sqrt{3}}{1+2\sin 2\alpha} \approx 0.1873$, below which the usual LSI cannot be violated. Namely, it can be concluded that there are no states violate the usual 3-setting LSI with the range of $\alpha \in [0, \frac{\arcsin \frac{\sqrt{3}-1}{2}}{2}]$. However, the 3-setting GLSI can detect more steerable states in the region of α and V , which can be calculated numerically.

See Fig. 4 and Fig. 5, for example, when $\alpha = \frac{\arcsin \frac{\sqrt{3}-1}{2}}{2} (\approx \frac{\pi}{17})$, there are no states violate the usual 3-setting LSI, however, the GLSI still can detect quantum states in the region $V \in [V_{\min} \approx 0.914, 1]$. In the range of $\alpha \in [\frac{\arcsin \frac{\sqrt{3}-1}{2}}{2}, \alpha_B], \alpha_B \approx 0.3508 \approx \frac{\pi}{9}$, there exist states violate the usual LSI, but the corresponding lower bound V_{\min} is larger than that of the 3-setting generalized LSI. In the range of $\alpha \in [\alpha_B, \frac{\pi}{4}]$, Both inequalities are almost equivalent in the task of steering test. Especially, when $\alpha = \frac{\pi}{4}$, both of them achieve $V_{\min} = \frac{\sqrt{3}}{3}$.

Example 3.—Let us consider the following asymmetric two-qubit mixed state [31]

$$\rho_2 = V|\Psi(\alpha)\rangle\langle\Psi(\alpha)| + (1-V)|\Phi(\alpha)\rangle\langle\Phi(\alpha)|, \quad (51)$$

where $|\Psi(\alpha)\rangle = \cos\alpha|HH\rangle + \sin\alpha|VV\rangle$ and $|\Phi(\alpha)\rangle = \sin\alpha|HV\rangle + \cos\alpha|VH\rangle$. Obviously, ρ_2 is entangled for the region of $\alpha \in (0, \pi/2)$, $V \in [0, 1/2) \cup (1/2, 1]$.

For the state Eq. (51), we come to compare the performance between the usual 3-setting LSI (Blue line) and the 3-setting GLSI (Red line) in Fig. 6. Because the state ρ_2 is unchanged under the following operations: $V \rightleftharpoons (1-V)$ and flipping Alice's states (i.e., $|H\rangle \rightleftharpoons |V\rangle$), thus the performance in the region $V \in (1/2, 1]$ will be the same as that in the region $V \in [0, 1/2)$. Without loss of generality, we choose the region of $\alpha \in (0, \pi/2)$, $V \in [0, 1/2)$, for the usual 3-setting LSI the upper bound $V_{\max} = \frac{1-\sqrt{3}+2\sin 2\alpha}{2(1+\sin 2\alpha)}$. It is obvious to conclude that there are no states violate the usual 3-setting LSI with the range of $\alpha \in [0, \frac{\arcsin \frac{\sqrt{3}-1}{2}}{2} \approx 0.1873]$. However, the 3-setting GLSI can detect some more steerable states for a wider region of α and V , which can be calculated numerically. See Fig. 6 and Fig. 7, for example, when $\alpha = \frac{\arcsin \frac{\sqrt{3}-1}{2}}{2} (\approx \frac{\pi}{17})$, there are no states violate the usual LSI, however, the GLSI still can detect quantum states in the region $V \in [0, V_{\max} \approx 0.0889]$. On the range of $\alpha \in [\frac{\arcsin \frac{\sqrt{3}-1}{2}}{2}, \alpha_B], \alpha_B \approx 0.4597 \approx \frac{5\pi}{34}$, there exist some states violate the usual 3-setting LSI, but the upper bound V_{\max} is lower than that of the 3-setting GLSI. On the range of $\alpha \in [\alpha_B, \frac{\pi}{4}]$, both inequalities are almost equivalent in the task of steering test. When $\alpha = \frac{\pi}{4}$, both of them achieve $V_{\max} = \frac{3-\sqrt{3}}{4}$.

APPENDIX C. EXPERIMENTAL DETAILS.

A 404nm laser is sent into a nonlinear crystal BBO to generate maximally entangled state of the form $|\phi\rangle = \frac{1}{\sqrt{2}}(|H\rangle_A|V\rangle_B - |V\rangle_A|H\rangle_B)$ with average fidelity over 99%. By setting HWP1 at 0° , the photon of Bob passes through BD1, which splits photon into two paths, upper (u) path and lower (l) path, according to its polarization, either vertical (V) and horizontal (H). If HWP2 is rotated by an angle $\frac{\beta}{2}$ and HWP3 is fixed at 45° , the two-photon entangled state becomes

$$|\Psi\rangle = \frac{\sin\beta}{\sqrt{2}}|H\rangle_A|H\rangle_{Bu} - \frac{\cos\beta}{\sqrt{2}}|H\rangle_A|V\rangle_{Bu} + \frac{1}{\sqrt{2}}|V\rangle_A|V\rangle_{Bl}, \quad (52)$$

where u and l donate upper path and lower path of Bob's photon, respectively. After that Bob's photon passes through BD2, the V -polarized element of the entangled state is lost in the upper path. One can verify that the matrix of the process of the asymmetric loss interferometer is

$$\begin{pmatrix} \sin\beta & 0 \\ 0 & 1 \end{pmatrix}, \quad (53)$$

Therefore, the final state (unnormalized state) is given by

$$|\Psi\rangle = \frac{\sin\beta}{\sqrt{2}}|H\rangle_A|H\rangle_B + \frac{1}{\sqrt{2}}|V\rangle_A|V\rangle_B. \quad (54)$$

After normalization, the two-qubit entangled state becomes

$$|\Psi\rangle = \frac{\sin\beta}{\sqrt{(\sin\beta)^2 + 1}}|H\rangle_A|H\rangle_B + \frac{1}{\sqrt{(\sin\beta)^2 + 1}}|V\rangle_A|V\rangle_B. \quad (55)$$

Compared with the form in the main text, by rotating HWP2 by $\beta = \arcsin(\sqrt{\frac{1}{(\sin\alpha)^2} - 1}) \cdot \frac{90}{\pi} \in [0, 45^\circ]$, we can generate

$$|\Psi\rangle = \cos\alpha|H\rangle_A|H\rangle_B + \sin\alpha|V\rangle_A|V\rangle_B. \quad (56)$$

In our experiments, the verification of the mixed state is achieved by probabilistically mixing the corresponding pure states. Specifically, we measured the corresponding observables in different pure states, and post-processed the data (change the probability of these pure states and mixing them together) to obtain experimental data of different mixed states. Now we show how to construct two types of mixed states, the generalized Werner state and a asymmetric mixed state [31],

$$\rho_1 = V|\Psi\rangle\langle\Psi| + (1 - V)\frac{\mathbb{1} \otimes \mathbb{1}}{4}, \quad (57)$$

$$\rho_2 = V|\Psi\rangle\langle\Psi| + (1 - V)|\Phi\rangle\langle\Phi|, \quad (58)$$

where $|\Phi\rangle = \sin\alpha|H\rangle_A|V\rangle_B + \cos\alpha|V\rangle_A|H\rangle_B$, and $V \in [0, 1]$ is the visibility (probability for $|\Psi\rangle\langle\Psi|$). The preparation of the maximally mixed state $\mathbb{1} \otimes \mathbb{1}$ is simulated by mixing the four states $|HH\rangle$, $|HV\rangle$, $|VH\rangle$, and $|VV\rangle$ with equal probability. The generalized Werner state is simulated by mixing $\mathbb{1} \otimes \mathbb{1}$ and $|\Psi\rangle\langle\Psi|$ with probability V and $1 - V$ respectively. The asymmetric mixed state is simulated by mixing $|\Psi\rangle$ and $|\Phi\rangle$ with probability V and $1 - V$ respectively. The specific rotation angles of HWP in the beam displacer interferometer for preparation these quantum states are shown in the table of Fig. 8.

FUNDING

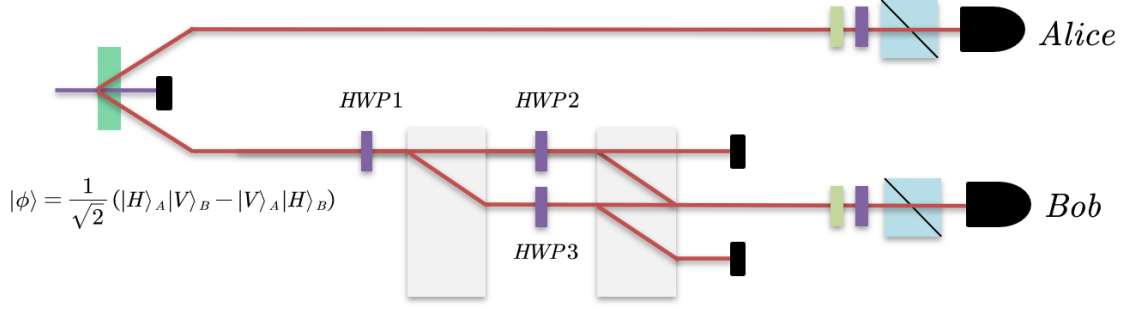
This work was supported by National Key R&D Program of China (2017YFA0305200, 2016YFA0301300), The Key R&D Program of Guangdong Province (2018B030329001, 2018B030325001), The National Natural Science Foundation of China (61974168, 12075245, 11875167, 12075001), and Xiaoxiang Scholars Programme of Hunan Normal university.

DISCLOSURES

The authors declare that there are no competing interests. T. Feng, C. R and Q. F contributed equally to this work.

REFERENCES

-
- * Electronic address: renchangliang@cigit.ac.cn
 † Electronic address: chenjl@nankai.edu.cn
 ‡ Electronic address: zhouxq8@mail.sysu.edu.cn
- [1] A. Einstein, B. Podolsky, and N. Rosen, “Can Quantum-Mechanical Description of Physical Reality Be Considered Complete?,” *Phys. Rev.* **47**, 777 (1935).
 - [2] E. Schrödinger, “Discussion of probability relations between separated systems,” *Naturwiss.* **23**, 807 (1935).
 - [3] H. M. Wiseman, S. J. Jones, and A. C. Doherty, “Steering, entanglement, nonlocality, and the Einstein-Podolsky-Rosen paradox,” *Phys. Rev. Lett.* **98**, 140402 (2007).
 - [4] J. S. Bell, “On the Einstein Podolsky Rosen Paradox,” *Physics (Long Island City, N.Y.)* **1**, 195 (1964).
 - [5] N. Brunner, D. Cavalcanti, S. Pironio, V. Scarani, and S. Wehner, “Bell nonlocality,” *Rev. Mod. Phys.* **86**, 419 (2014).
 - [6] J. Clauser, M. Horne, A. Shimony, and R. Holt, “Proposed Experiment to Test Local Hidden-Variable Theories,” *Phys. Rev. Lett.* **23**, 880 (1969).
 - [7] N. D. Mermin, “Extreme quantum entanglement in a superposition of macroscopically distinct states,” *Phys. Rev. Lett.* **65**, 1838 (1990).
 - [8] D. Collins, N. Gisin, N. Linden, S. Massar, and S. Popescu, “Bell Inequalities for Arbitrarily High-Dimensional Systems,” *Phys. Rev. Lett.* **88**, 040404 (2002).
 - [9] D. M. Greenberger, M. A. Horne, and A. Zeilinger, in *Bell’s Theorem, Quantum Theory, and Conceptions of the Universe*, edited by M. Kafatos (Kluwer, Dordrecht, 1989), p. 69.
 - [10] L. Hardy, “Nonlocality for Two Particles without Inequalities for Almost All Entangled States,” *Phys. Rev. Lett.* **71**, 1665 (1993).
 - [11] A. Aspect, P. Grangier, and G. Roger, “Experimental Tests of Realistic Local Theories via Bell’s Theorem,” *Phys. Rev. Lett.* **47**, 460 (1981).
 - [12] J. W. Pan, D. Bouwmeester, M. Daniell, H. Weinfurter, and A. Zeilinger, “Experimental test of quantum nonlocality in three-photon Greenberger–Horne–Zeilinger entanglement,” *Nature (London)* **403**, 515 (2000).
 - [13] Y. H. Luo *et al.*, “Experimental Test of Generalized Hardy’s Paradox,” *Sci. Bull.* **63**, 1611 (2018).
 - [14] M. D. Reid, P. D. Drummond, E. G. Cavalcanti, W. P. Bowen, P. K. Lam, H. A. Bachor, et al. “The Einstein-Podolsky-Rosen paradox: From concepts to applications,” *Reviews of Modern Physics*, **81**(25), 1727 (2009).
 - [15] D. J. Saunders, S. J. Jones, H. M. Wiseman, and G. J. Pryde, “Experimental EPR-steering using Bell-local states,” *Nat. Phys.* **6**, 845-849 (2010).
 - [16] K. Sun, J. S. Xu, X. J. Ye, Y. C. Wu, J. L. Chen, C. F. Li, and G. C. Guo, “Experimental Demonstration of the Einstein-Podolsky-Rosen Steering Game Based on the All-Versus-Nothing Proof,” *Phys. Rev. Lett.* **113**, 140402 (2014).
 - [17] S. Armstrong, M. Wang, R. Y. Teh, Q. H. Gong, Q. Y. He, J. Janousek, H. A. Bachor, M. D. Reid, and P. K. Lam, “Multipartite Einstein-Podolsky-Rosen steering and genuine tripartite entanglement with optical networks,” *Nature Phys.* **11**, 167 (2015).
 - [18] A. J. Bennet, D. A. Evans, D. J. Saunders, C. Branciard, E. G. Cavalcanti, H. M. Wiseman, and G. J. Pryde, “Arbitrarily Loss-



$ H\rangle = 0\rangle; V\rangle = 1\rangle$	HWP1	HWP2	HWP3
$\cos\alpha 0\rangle_A 0\rangle_B + \sin\alpha 1\rangle_A 1\rangle_B$	0°	$\arcsin\left(\sqrt{\frac{1}{\sin^2\alpha}-1}\right) \cdot \frac{90}{\pi} \in [0, 45^\circ]$	45°
$ 0\rangle_A 0\rangle_B$	0°	45°	0°
$ 0\rangle_A 1\rangle_B$	45°	0°	45°
$ 1\rangle_A 0\rangle_B$	45°	45°	0°
$ 1\rangle_A 1\rangle_B$	0°	0°	45°
$\sin\alpha 0\rangle_A 1\rangle_B + \cos\alpha 1\rangle_A 0\rangle_B$	45°	$\arcsin\left(\sqrt{\frac{1}{\sin^2\alpha}-1}\right) \cdot \frac{90}{\pi} \in [45^\circ, 90^\circ]$	

FIG. 8: The experimental setup and the specific angles for state preparation.

Tolerant Einstein-Podolsky-Rosen Steering Allowing a Demonstration over 1 km of Optical Fiber with No Detection Loop-hole,” *Phys. Rev. X* **2**, 031003 (2012).

- [19] J. Schneeloch, P. B. Dixon, G. A. Howland, C. J. Broadbent, and J. C. Howell, “Violation of Continuous-Variable Einstein-Podolsky-Rosen Steering with Discrete Measurements,” *Phys. Rev. Lett.* **110**, 130407 (2013).
- [20] M. Fadel, T. Zibold, B. Decamps, P. Treutlein, “Spatial entanglement patterns and Einstein-Podolsky-Rosen steering in Bose-Einstein condensates,” *Science* **360**, 409-413 (2018).
- [21] F. Dolde, I. Jakobi, B. Naydenov, N. Zhao, S. Pezzagna, C. Trautmann, J. Meijer, P. Neumann, F. Jelezko, and J. Wrachtrup, “Room-temperature entanglement between single defect spins in diamond,” *Nat. Phys.* **9**, 139-143 (2013).
- [22] M. Dabrowski, M. Parniak, and W. Wasilewski, “Einstein-Podolsky-Rosen paradox in a hybrid bipartite system,” *Optica* **4**, 272-275 (2017).
- [23] D. Cavalcanti, P. Skrzypczyk, G. H. Aguilar, R. V. Nery, P. H. S. Ribeiro, and S. P. Walborn, “Detection of entanglement in asymmetric quantum networks and multipartite quantum steering,” *Nat. Commun.* **6**, 7941 (2015).
- [24] Q. Zeng, B. Wang, P. Li, and X. Zhang “Experimental High-Dimensional Einstein-Podolsky-Rosen Steering,” *Phys. Rev. Lett.* **120**, 030401 (2018).
- [25] J. L. Chen, H. Y. Su, Z. P. Xu, and A. K. Pati, “Sharp Contradiction for Local- Hidden-State Model in Quantum Steering,” *Sci. Rep.* **6**, 32075 (2016).
- [26] N. D. Mermin, “Quantum mysteries refined,” *Am. J. Phys.* **62**, 880 (1994).
- [27] S. H. Jiang, Z. P. Xu, H. Y. Su, A. K. Pati, and J. L. Chen, “Generalized Hardy’s Paradox,” *Phys. Rev. Lett.* **120**, 050403 (2018).
- [28] For example, the maximal violation value for the usual 3-setting steering inequality (9) is $1 + 2 \sin 2\alpha$. Hence, only when $\alpha > \frac{\arcsin \frac{\sqrt{3}-1}{2}}{2} \approx 0.1873$, the usual linear steering inequality can be violated. However, the pure state violates the GLSI (8) for the whole region $\alpha \in (0, \pi/2)$, thus the GLSI is stronger than the usual LSI in detecting the EPR steerability of pure entangled states.
- [29] P. G. Kwiat, K. Mattle, H. Weinfurter, and A. Zeilinger, “New High-Intensity Source of Polarization-Entangled Photon Pairs,” *Phys. Rev. Lett.* **75**, 4337 (1995).
- [30] E. Wigner, “On the quantum correction for thermodynamic equilibrium”, *Phys. Rev.*, **40**, 749 (1932).
- [31] J. L. Chen, X. J. Ye, C. Wu, H. Y. Su, A. Cabello, L. C. Kwek, and C. H. Oh, “All-versus-nothing proof of Einstein-Podolsky-Rosen steering”, *Sci. Rep.* **3**, 02143 (2013).
- [32] R. Uola, A. C. S. Costa, H. C. Nguyen, and O. Gühne, “Quantum steering,” *Rev. Mod. Phys.* **92**, 015001 (2020).
- [33] C. Branciard, E. G. Cavalcanti, S. P. Walborn, V. Scarani, and H. M. Wiseman, “One-sided device-independent quantum key distribution: Security, feasibility, and the connection with steering,” *Phys. Rev. A* **85**, 010301 (2012).
- [34] P. Skrzypczyk and D. Cavalcanti, “Maximal Randomness Generation from Steering Inequality Violations Using Qudits,”

- Phys. Rev. Lett. **120**, 260401 (2018).
- [35] Y. Guo, S. Cheng, X. Hu, B. Liu, E. Huang, Y. Huang, C. Li, G. Guo, and E. G. Cavalcanti, “Experimental Measurement-Device-Independent Quantum Steering and Randomness Generation Beyond Qubits,” Phys. Rev. Lett. **123**, 170402 (2019).
- [36] M. Piani and J. Watrous, “Necessary and Sufficient Quantum Information Characterization of Einstein-Podolsky-Rosen Steering,” Phys. Rev. Lett. **114**, 060404 (2015).
- [37] K. Sun, X. Ye, Y. Xiao, X. Xu, Y. Wu, J. Xu, J. Chen, C. Li and G. Guo, “Demonstration of Einstein-Podolsky-Rosen steering with enhanced subchannel discrimination,” npj Quantum Inf. **4**, 12 (2018).